



1 *Conference Proceedings Paper*

2 **Radiometric Calibration of RapidScat using GPM** 3 **Microwave Imager**

4 **Ali Al-Sabbagh*, Ruaa Alsabah, and Josko Zec**

5 Department of Electrical and Computer Engineering, Florida Institute of Technology, Melbourne 32901, FL,
6 USA; aalsabbagh2014@my.fit.edu (A.A.); ralsabah2014@my.fit.edu (R.A.); jzec@fit.edu (J.Z.).

7 * Correspondence: aalsabbagh2014@my.fit.edu;

8 Published: date

9 Academic Editor: name

10 **Abstract:** Flying in a non-Sun-synchronous orbit, RapidScat is the first scatterometer capable of
11 measuring ocean vector winds over the full diurnal cycle, instead of observing a given location at a
12 fixed time of day. Non-Sun-synchronous orbit also enables the overlap with other satellite
13 instruments that have been flying in Sun-synchronous orbits. RapidScat covered the latitude range
14 between $\pm 51.6^\circ$ and was operated on-board the International Space Station between September
15 2014 and August 2016. This paper describes the process that combines RapidScat's active and
16 passive modes, simultaneously measuring both the radar surface backscatter (active mode), and the
17 microwave emission determining the system noise temperature (passive mode). This work also
18 presents the radiometric (passive mode) cross-calibration using the GPM Microwave Imager (GMI)
19 as a reference to eliminate the measurement biases of brightness temperature between a pair of
20 radiometer channels that are operating at slightly different frequencies and incidence angles. Since
21 the RapidScat operates at 13.4 GHz and the closest GMI channel is 10.65 GHz, GMI brightness
22 temperatures were normalized before the calibration. Normalization was based on the radiative
23 transfer model (RTM) to yield an equivalent brightness temperature prior to direct comparison with
24 RapidScat. The seasonal and systematic biases between two radiometers have been calculated for
25 both polarizations as a function of geometry, atmospheric and ocean brightness temperature
26 models. Calculated biases may be used for measurement correction and for reprocessing of
27 geophysical retrievals.

28 **Keywords:** RapidScat; GPM Imager; radiometric calibration; brightness temperature.

29 **1. Introduction**

30 The RapidScat (RS) scatterometer was launched in Sept. 2014 installed on the Columbus module
31 of the International Space Station (ISS). It started making measurements over the Earth's surface in
32 Oct. 2014 and continued until Aug. 2016. The instrument operated in a manner similar to QuikScat,
33 a previous Ku-band scatterometer, as NASA had used the QuikScat's spare engineering unit to build
34 the follow-up RapidScat instrument [1-3]. RapidScat is a dual beam, conical-scanning, long-pulse
35 radar system. It combines active and passive Ku-band microwave measurements in dual receiver
36 channels. The backscatter is measured in a narrowband channel, and the brightness temperature (Tb)
37 in a wider-band channel, both from the ocean surface and through the intervening atmosphere
38 [4]. The primary use of scatterometer measurements is wind vector retrieval over sea surface. In the
39 passive mode, the RapidScat measures the linearly polarized microwave emission at 13.4GHz
40 frequency quantified by Tb. The rotating antenna generated vertically (VV) and horizontally (HH)
41 polarized beams directed at the Earth's surface at incidence angles of approximately 56° and 49° ,
42 respectively. The ground swath of the outer VV beam is approximately 1100km wide, while the
43 ground swath of the inner HH beam is approximately 900km wide. Regions between $\pm 58^\circ$ latitude

44 are sampled uniformly over 24-hour periods, as opposed to previous Sun-synchronous scatterometer
45 orbits with fixed diurnal sampling flying over the same land areas at the same time of day [5-8]. This
46 paper presents the first radiometric calibration work of RapidScat brightness temperature
47 measurements over oceans. To accomplish the calibration, Radiative Transfer Model (RTM),
48 developed at the Central Florida Remote Sensing Laboratory (CRFSL) [9], was used to evaluate the
49 corresponding modeled brightness temperatures. The RTM uses the collocated environmental
50 parameters (surface truth) and given sensor parameters (incidence angle, frequency, and
51 polarization), to produce the simulated Tb. In addition, in comparison with the RTM model, GPM
52 Imager measurements are used for radiometer cross-calibration. To facilitate the cross-calibration,
53 the GMI brightness temperatures are translated to yield an equivalent Tb prior to direct comparison
54 with RapidScat using the RTM. The Tb differences were analyzed seasonally as a function of ocean
55 brightness temperature and atmospheric models.

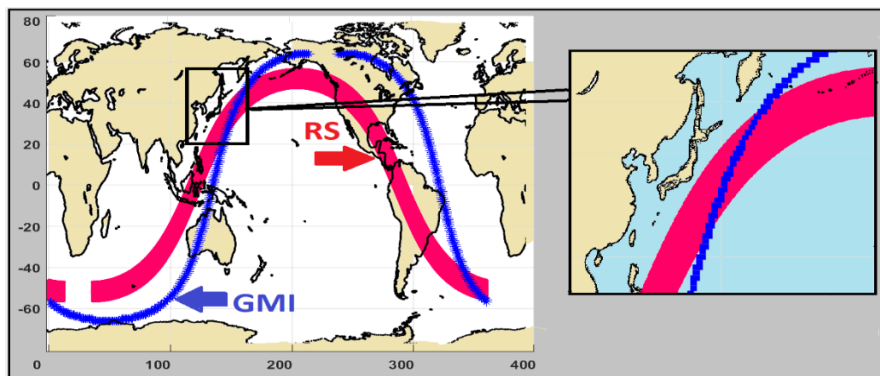
56 2. Materials and Calibration Method

57 In this work, RapidScat data have been extracted from the Level 2A (L2A) and Level 2B (L2B).
58 The data products were generated by the Physical Oceanography Distributed Active Archive Center
59 (PODAAC) at the Jet Propulsion Laboratory [10]. Data products come in three versions, 1.1, 1.2, and
60 1.3, with 1.2 replacing 1.1 after 8/15/2015; version 1.3 is intended as a replacement and continuation
61 of the Version 1.1 and Version 1.2 data from 02/11/2016 [11]. For the Tb modeling, the surface truth
62 parameters were extracted from the Global Data Assimilation System (GDAS) data product. GDAS
63 global grids are updated every six hours at 0:00, 6:00, 12:00, and 18:00 UTC. Parameters listed in
64 GDAS file include temperature, surface pressure, humidity, cloud liquid water, sea surface
65 temperature, and wind vectors [12].

66 The goal of the radiative transfer model (RTM) is to calculate the brightness temperature at
67 the defined operating frequency and incidence angle. The RTM is used in this work to generate Tb at
68 13.4 GHz; then, global measured and modeled RapidScat Tb's can be compared for both
69 polarizations. The environmental parameters of the ocean and atmosphere were prepared for the
70 input to the RTM. The most important characteristic of the RTM is that it accurately captures the
71 dynamics of the ocean Tb and environmental parameters. The three main RTM components that
72 contribute to the Tb captured by a space-borne sensor are the apparent brightness temperature from
73 radiometer measurements, the ocean surface brightness temperature, and the ocean surface which
74 reflects the sky brightness with some loss. This is an incoherent summation from the atmosphere and
75 surface [4, 9].

76 Examples of RapidScat and GMI orbits mapped over the globe are illustrated in Fig. 1. It shows
77 a wide RapidScat swath in red, and the GMI orbit in blue. The wide RapidScat swath in Sun-
78 asynchronous orbit allows collocation at different latitudes. For each collocated (RapidScat / GMI)
79 data, there must be corresponding GDAS parameters within a ± 60 minute window. This temporal
80 criterion eliminates about 2/3 or all data for which GDAS reference may not be valid (4 GDAS daily
81 files spanning total 8-hour window to collocate with satellites).

82



83
84

Figure 1. RapidScat / GPM Imager collocations.

85 The collocated (RS/GMI) brightness temperatures over a two-year period have a wide
 86 geographic coverage for ascending and descending passes. To ensure high quality
 87 calibration/validation, this data set was spatially selected within 1° latitude x longitude boxes, using
 88 a conservative land, rain, and a heavy cloud mask. These boxes were quality controlled and edited
 89 to remove non-homogenous ocean scenes and/or transient environmental conditions. Rain flag and
 90 rain impact from L2B were used to remove any 1° box with a rain rate higher than zero, and when
 91 the GDAS indicated high water vapor (> 60 mm). The final valid data set now consists of the
 92 environmental parameters (GDAS) with incidence angle and measured vertical and horizontal Tbs
 93 (from L2A). Next, the RapidScat brightness temperature has been compared to the GMI. The purpose
 94 of this technique was to find a radiometric calibration bias from one radiometer to another, and thus
 95 to reduce the relative biases among the sensors [13].

96 The GMI is a non-sun-synchronous, dual-polarization, conical-scanning, multi-channel (ranging
 97 from 10 to 183 GHz) radiometer, and it makes calibrated measurements at different wavelengths and
 98 polarizations [14]. For the Imager, the two lowest frequency channels at 10.65 GHz and 18.7 GHz
 99 bracket the RapidScat at 13.4 GHz; however, the incidence angles do not match. The GMI incidence
 100 angle is 52.8° for all channels; however, for RapidScat, the inner (H-pol) beam is 46°, and the outer
 101 (V-pol) beam is 54°. Thus, GMI Tbs are translated to yield an equivalent Tb prior to direct comparison
 102 with RapidScat [15, 16]. The radiative transfer model is used to calculate the equivalent RS Tbs from
 103 GMI channels (10.65 and 18.7 GHz), to produce the equivalent 13.4 GHz at the corresponding
 104 RapidScat incidence angles. This process involved using a spectral ratio (S_r) parameter for both
 105 polarizations calculated as a function of water vapor, cloud liquid water, and sea surface
 106 temperature, which is defined by Equation 1:

$$S_r(wv, clw, sst) = \frac{RS_{rtm13.4} - GMI_{rtm10.65}}{GMI_{rtm18.7} - GMI_{rtm10.65}} \quad (1)$$

107
 108 Where $RS_{rtm13.4}$, $GMI_{rtm10.65}$, and $GMI_{rtm18.7}$ are the modeled brightness temperatures for RS and
 109 GMI, respectively [17, 18]. Using this ratio, the GMI brightness temperatures (10.65 and 18.7 GHz)
 110 were translated to the RapidScat equivalent Tb (13.4 GHz) as shown in Equation 2:

$$Tb_{GMI_{13.4}} = Tb_{GMI_{10.65}} + S_r (Tb_{GMI_{18.7}} - Tb_{GMI_{10.65}}) \quad (2)$$

111
 112 Where $Tb_{GMI_{10.65}}$, and $Tb_{GMI_{18.7}}$ are the observed brightness temperatures. By having the
 113 equivalent 13.4 GHz Tb's (TB GMI eqv), the difference between the observed RapidScat and the
 114 equivalent GMI Tb's can be calculated by the Equation 3. Figure 2 summarizes the calibration
 115 procedure in a block diagram.

$$Tb_{Dif} = Tb_{RS_{obs}} - Tb_{GMI_{eqv}} \quad (3)$$

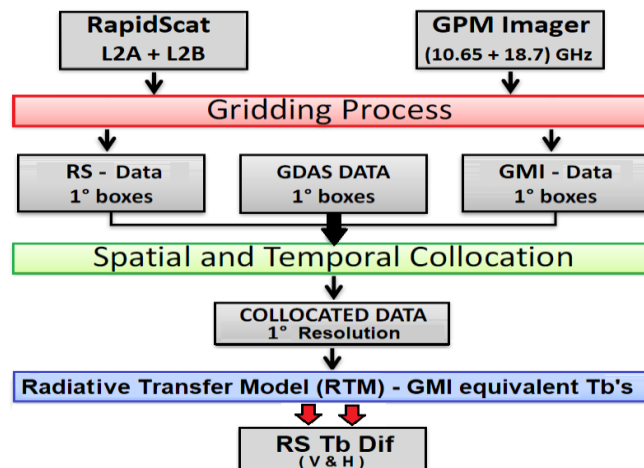
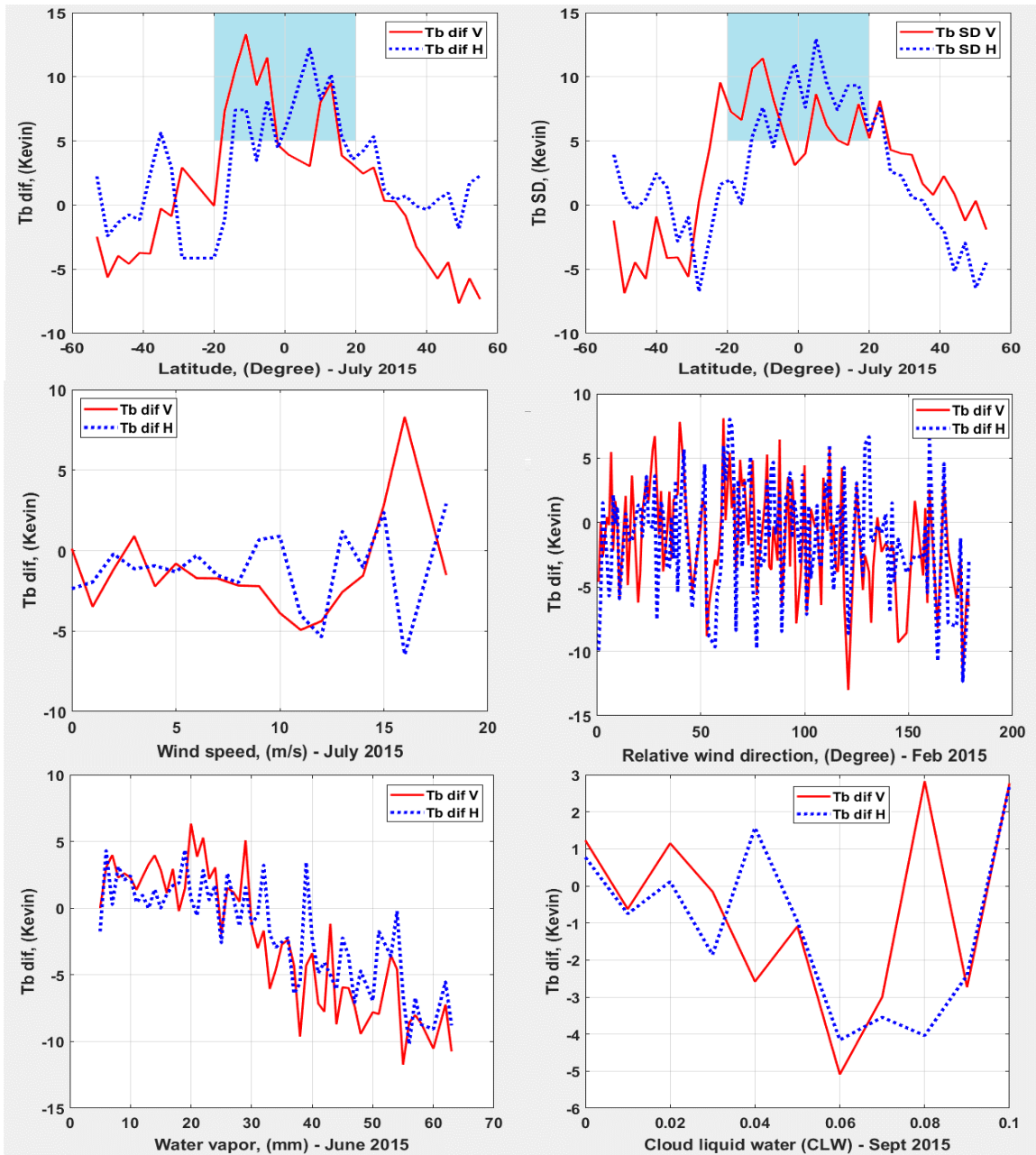


Figure 2. Radiometric Calibration Process.

136 **3. Results**

137 This section presents RapidScat/GMI Tb differences in arbitrary selected periods between
 138 January 2015 and August 2016. To assess the Tb difference affected by each parameter, geometry and
 139 environmental factors were precisely examined. In each of the processed data sets overall agreement
 140 between both polarizations is observed. Figure 3 summarizes the Tb differences as a function of wind
 141 speed in July 2015, relative wind direction in Feb. 2015, water vapor in June 2015, and cloud liquid
 142 water in Sept. 2015. In addition to the atmospheric and ocean brightness temperature models, latitude
 143 dependency was also investigated, as shown for July 2015. The horizontal axis represents the latitude
 144 over the oceans from 55° latitude-south to 55° north (collocation region). The second and bottom
 145 windows present the average RapidScat/GMI Tb differences separated in horizontal (blue line) and
 146 vertical (red line) polarizations.
 147

148



149

150

151

152

Figure 3. Tb differences/biases as a function of latitude (top), Tb differences as a function of wind speed, relative wind direction (middle), and water vapor, and cloud liquid water (bottom).

153 **4. Discussion**

154 To present latitude dependency, averages over longitude, known as *zonal averages*, were
155 performed to form a latitude series (to reduce the Tb measurement standard deviation). The top panel
156 shows the averaged Tb differences of RapidScat/GMI (left), while the right panel presents the
157 RapidScat Tb biases for both beams (Single Difference (SD): Tb measured – Tb modeled). It is
158 noticeable that the highest differences were recorded in the same region between -20° to 20° latitude
159 for both polarizations, as shown in the shaded area.

160 To evaluate RapidScat/GMI differences as a function of latitude, Tb difference dependence on
161 wind speed (left) and relative wind direction (right) was investigated for both beams and presented
162 in the second row. The difference variation changes in most circumstances are within $\pm 3\text{K}$; however,
163 there is an exception, especially for wind speeds above 10 m/s where the Tb difference became higher.
164 Moreover, the right panel captures the average Tb differences as a function of the relative wind
165 direction. Differences at both polarizations follow the same pattern, and all the radiometric measured
166 data in 2015 shows good overall average agreement in both inner and outer beams, with the red and
167 blue lines presenting the averaged Tb differences in inner and outer beam, respectively.

168 The other environmental factor that was examined is the water vapor. The presence of water
169 vapor in the atmosphere causes an increase in the brightness temperatures measured by microwave
170 instruments. The bottom panel (left) illustrates an example for June 2015. The examined periods show
171 a good agreement between the inner and the outer beam, but the Tb difference changes behavior
172 from positive to negative when the water vapor exceeds 25 mm in both polarizations. Additionally,
173 an analysis of the Tb differences versus the cloud liquid water (CLW) was examined. The plot on the
174 right shows the Tb differences mostly within $\pm 2\text{K}$, except for the CLW higher than 0.05 mm for both
175 beams.

176 **5. Conclusions**

177 This paper describes the RapidScat's passive mode with radiometer measurements to obtain the
178 brightness temperature simultaneously with primary active mode collecting normalized radar cross
179 section measurements. This work presents differences between RapidScat and the GPM Imager
180 measured Tbs as a function of the main RTM environmental inputs. Wind Speed, relative wind
181 direction, water vapor, and cloud liquid water are four major factors that affect microwave apparent
182 brightness temperatures. To understand their contribution to the RapidScat Tb bias, those
183 environmental factors were examined. The trends of the Tb deviation could be studied by this method
184 to assess the Tb bias affected by each parameter.

185 Results obtained from two years of observations indicate that most of the measured data in 2015
186 show good overall average agreement. Also, it can be concluded that RapidScat brightness
187 temperature is a reliable source of data and it satisfies the accuracy requirements, despite Tb not
188 being RapidScat's primary data product. Data used in the validation were collected from the entire
189 RapidScat's mission. Further analysis of the RapidScat measurement set may help estimate relative
190 validity and stability of other scatterometers/radiometers.

191

192 **Acknowledgments:** This research was performed under the grant NNX15AT70G from the NASA Headquarters.
193 Both L2A and L2B RapidScat data sets were provided by the NASA Physical Oceanography Distributed Active
194 Archive Center (PODAAC) at the Jet Propulsion Laboratory (<https://podaac.jpl.nasa.gov/>). The authors also wish
195 to acknowledge the collaboration with Prof. W. Linwood Jones at Central Florida Remote Sensing Laboratory,
196 University of Central Florida.

197 **Author Contributions:** This research was designed and guided by Dr. Josko Zec. Ali Al-Sabbagh and Ruaa
198 Alsabah performed, analyzed, and discussed the research data. All authors helped in improving this paper.

199 **Conflicts of Interest:** The authors declare no conflict of interest.

200

201 **References**

- 202 1. Josko Zec, W.L.Jones, Ruaa Alsabah, and Ali Al-Sabbagh. "RapidScat Cross-Calibration Using the Double
203 Difference Technique." *Remote Sens.* 2017, 9, 1160.
- 204 2. Ruaa Alsabah, Ali Al-Sabbagh, and Josko Zec. "Calibration of RapidScat scatterometer." In *Microwaves,
205 Radar and Remote Sensing Symposium (MRRS), 2017 IEEE*, pp. 249-252. IEEE, 2017.
- 206 3. Ali Al-Sabbagh, Ruaa Alsabah, and Josko Zec, "Calibration of RapidScat Brightness Temperature" MIT-
207 15th meeting of Microwave Radiometry and Remote Sensing of the Environment (MicroRad), Cambridge,
208 MA, USA, March, 2018.
- 209 4. Jones, W. Linwood, Rushad Meher Shahi, Josko Zec, and David G. Long. "SeaWinds on QuikSCAT
210 radiometric measurements and calibration." In *Geoscience and Remote Sensing Symposium, 2000.
211 Proceedings. IGARSS 2000. IEEE 2000 International*, vol. 3, pp. 1027-1029. IEEE, 2000.
- 212 5. Durden, Stephen L., and Dragana Perkovic-Martin. "The RapidScat Ocean Winds Scatterometer: A Radar
213 System Engineering Perspective." *IEEE Geoscience and Remote Sensing Magazine* 5, no. 3 (2017).
- 214 6. Wentz, Frank J., Lucrezia Ricciardulli, Ernesto Rodriguez, Bryan W. Stiles, Mark A. Bourassa, David G.
215 Long, Ross N. Hoffman et al. "Evaluating and extending the ocean wind climate data record." *IEEE Journal
216 of Selected Topics in Applied Earth Observations and Remote Sensing* 10, no. 5 (2017): 2165-2185.
- 217 7. Paget, C.A.; Long, G.D.; Madsen, N.M. RapidScat Diurnal Cycles Over Land. *IEEE Trans. Geosci. Remote
218 Sens.* 2016, 54, 3336–3344.
- 219 8. Madsen, Nathan M., and David G. Long. "Calibration and validation of the RapidScat scatterometer using
220 tropical rainforests." *IEEE Transactions on Geoscience and Remote Sensing* 54.5 (2016): 2846-2854.
- 221 9. Biswas; K,S.; Farrar, S.; Gopalan, K.; Santos-Garcia, A.; Jones, W.L.; Bilanow, S. Intercalibration of
222 microwave radiometer brightness temperatures for the global precipitation measurement mission. *IEEE
223 Trans. Geosci. Remote Sens.* 2013, 51, 1465–1477.
- 224 10. Shen, Y. ISS-RapidSca. 2015. Available online:
225 https://www.nasa.gov/mission_pages/station/research/experiments/1067.html (accessed on 20 July 2016).
- 226 11. RapidScat Project. 2016. RapidScat Level 2A Surface Flagged Sigma-0 and Attenuations in 12.5Km Swath
227 Grid Version 1.2. Ver. 1.2. PO.DAAC, CA, USA. Available online: <http://dx.doi.org/10.5067/RXS12-L2A12>
228 (accessed on 20 July 2016).
- 229 12. Climate Prediction Center. National Centers for Environmental Prediction. National Oceanic and
230 Atmospheric Administration (NOAA). Available online: <http://www.ncep.noaa.gov/> (accessed on 20 July
231 2016).
- 232 13. Hanna, Rafik, "Validation of QuickSCAT radiometer (QRad) microwave brightness temperature
233 measurements", PhD diss., University of Central Florida, 2009.
- 234 14. Chen, Ruiyao, Hamideh Ebrahimi, and W. Linwood Jones. "Creating a Multidecadal Ocean Microwave
235 Brightness Dataset: Three-Way Intersatellite Radiometric Calibration Among GMI, TMI, and
236 WindSat." *IEEE Journal of Selected Topics in Applied Earth Observations and Remote Sensing* 10, no. 6
237 (2017): 2623-2630.
- 238 15. Hanna, Rafik, and W. Linwood Jones. "Brightness temperature validation for SeaWinds radiometer using
239 Advanced Microwave Scanning Radiometer on ADEOS-II." *Geoscience and Remote Sensing Symposium,
240 2007. IGARSS 2007. IEEE International. IEEE, 2007.*
- 241 16. Hanna, Rafik, and Linwood Jones. "Inter-Satellite Radiometric Calibration for a Satellite Radar
242 Scatterometer." *Proc. of SPIE Vol. Vol. 7691*. 2010.
- 243 17. Rastogi, Mayank, W. Linwood Jones, Jun D. Park, and Ian Adams. "Seawinds radiometer (SRad) on
244 ADEOS-II brightness temperature calibration/validation." In *Geoscience and Remote Sensing Symposium,
245 2005. IGARSS'05. Proceedings. 2005 IEEE International*, vol. 5, pp. 3441-3444. IEEE, 2005
- 246 18. Rastogi, Mayank, W. Linwood Jones, and Ian Adams. "SeaWinds radiometer (SRad) brightness
247 temperature calibration and validation." In *SoutheastCon, 2005. Proceedings. IEEE*, pp. 287-295. IEEE, 2005.

